Reproducible Surface-Enhanced Raman Quantification of Biomarkers in Multicomponent Mixtures

Anna Chiara De Luca,[†,*] Peter Reader-Harris,[‡] Michael Mazilu,[‡] Stefania Mariggiò,[†] Daniela Corda,[†] and Andrea Di Falco[‡,*]

[†]Institute of Protein Biochemistry, National Research Council, Via P. Castellino 111, 80131 Naples, Italy and [‡]SUPA, School of Physics and Astronomy, University of St. Andrews, North Haugh, KY16 9SS St. Andrews, United Kingdom

ABSTRACT Direct and quantitative detection of unlabeled glycerophosphoinositol (GroPIns), an abundant cytosolic phosphoinositide derivative, would allow rapid evaluation of several malignant cell transformations. Here we report label-free analysis of GroPIns *via* surface-enhanced Raman spectroscopy (SERS) with a sensitivity of 200 nM, well below its apparent concentration in cells. Crucially, our SERS substrates, based on lithographically defined gold nanofeatures, can be used to predict accurately the GroPIns concentration even in multicomponent mixtures, avoiding the preliminary separation of individual compounds. Our results represent a critical step toward the creation of SERS-based biosensor for rapid, label-free, and reproducible detection of specific molecules, overcoming limits of current experimental methods.

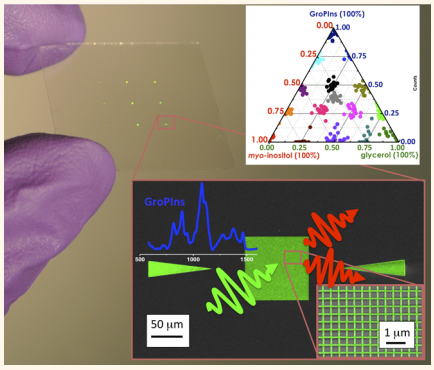

KEYWORDS: SERS · biosensor · glycerophosphoinositol · nanofabrication · label-free detection

Glycerophosphoinositol (GroPIns) is an abundant component of cell cytosol, produced by $PLA_2IV\alpha$ hydrolysis of membrane phosphatidylinositol, that regulates important biological functions, among which are cell proliferation and differentiation.[1−3] GroPIns gained attention as a potential active metabolite when its cellular levels were associated with oncogenic Ras transformation in epithelial cells.[1,2] Ras genes encode proteins involved in signal transduction within cells, and their mutations and amplifications can lead to cancer.[4] Subsequently, GroPIns presence and potential tumor-related functions became apparent in several other cell lines, including thyroid cells transformed by oncogenes responsible for papillary thyroid carcinomas.[5] Recent evidence highlights the potential role of GroPIns during the immune cell responses.[6,7] These studies led to the proposal that GroPIns cellular levels can be considered a biochemical marker of patho/physiological conditions.

Currently, the techniques used for GroPIns detection are [^{3}H]-*myo*-inositol equilibrium radio labeling followed by HPLC analysis or mass spectroscopy.[8] The first method requires radioactive labeling, and sometimes the low specific activity renders the comparisons across multicomponent mixtures extremely difficult.[2] Conversely, mass spectroscopy is a label-free method and has generated most of the valuable evidence for the physiological relevance of GroPIns.[1,9] However, this method is time-consuming and requires an efficient chromatographic separation in order to achieve mass analysis. Moreover, a large quantity of sample needs to be processed for an efficient quantitative analysis, enabling only an estimation of the mean amount of GroPIns (expressed in pmol/cell) in a cell population.[8,9] This led to an increased interest in developing alternative molecular technologies allowing the sensitive and quantitative detection of minimal GroPIns concentration sample, avoiding time-consuming sample preparation or need of label/dye.

Raman scattering, due to its fingerprint-like nature, allows the detection and characterization of biomolecules.[10,11] Unfortunately, typical Raman cross sections are very small: only one photon in a million is Raman

* Address correspondence to a.deluca@ibp.cnr.it, adf10@st-andrews.ac.uk.

Received for review December 2, 2013 and accepted February 13, 2014.

Published online February 13, 2014
10.1021/nn406200y

scattered by the molecule of interest. However, the efficiency of the scattering can be dramatically enhanced, up to single-molecule detection levels, by exploiting the field enhancement in the presence of metallic nanostructured surfaces. This approach corresponds to surface-enhanced Raman scattering (SERS). Since its discovery in 1974 by Fleishman,[12] SERS has been used for studies of very low concentrations of analytes in different chemical environments.[13−18] It is a truly label-free technique, in that it does not require any dye/marker or specific treatment of the substrates to grant specificity to the analysis. In the SERS experiments, the incoming laser beam interacts with the electron plasma oscillations in the metallic nanostructures to enhance, by multiple orders of magnitude, the vibrational spectra of molecules adsorbed or close to the surface.[19−21] Therefore, the SERS substrate plays a crucial role, and the widespread use of SERS has been hampered by the substrate's sensitivity and reproducibility.[22] The sensitivity refers to the detection capability of low concentration of molecules. Reproducibility refers to the ability to allow quantitative and repeatable measurements for independent realizations in similar conditions. This is a highly critical requirement since most of the SERS-based sensing relies on the relative intensity of specific Raman frequency bands.[23,24]

Much of the development effort of SERS substrates has been focused on increasing the absolute sensitivity aiming for single-molecule detection. The most popular approach is to use high-field intensity produced by clustered silver (Ag) nanoparticles in nanocolloidal (NC) solutions.[18,25] This method is cheap and gives high efficiencies; however, it is limited by oxidation, laser-induced structural changes in the silver oxide layers, and a nonuniform and random distribution of hot spots.[17] Additionally, single-molecule detection needs the *a priori* knowledge of the exact location of the hot spot. Other geometries, mainly made by top-down lithographic approaches, allow tailoring the field enhancement and its spatial distribution[26−32] and have unlocked the use of SERS for single-molecule detection.[33−35]

However, in most practical applications, experiments are run at intermediate concentration regimes where the analyte covers large areas of the substrate. In this case, it is more convenient to have an extended distribution of field enhancement, rather than a sparse collection of high intensity hot spots, as pointed out in previous works.[22,36,37] Here, we show how a simple Au-fishnet nanostructure on a chemically inert substrate (microscope glass slide) allows unprecedented reproducibility in sensing of test molecules (Rd6G, at a concentration of 10^{-8} M) and even molecules of biological interests (GroPIns, at concentrations of 10 mM to 200 nM). We compared the performance of Au-fishnet substrates to conventional colloidal

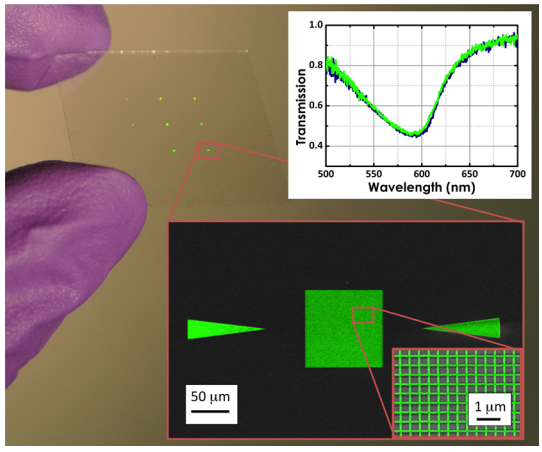

Figure 1. Photo of SERS substrate and zoomed scanning electron microscope (SEM) image of typical Au-fishnet pad. Transmission spectra of a typical SERS pad (blue and green show the two polarizations).

nanoparticles, crucially demonstrating an improvement of the reproducibility without a penalizing reduction of efficiency. We exploited this quality of the SERS measurements to perform the first quantitative GroPIns sensing at concentrations close to physiological conditions. In this context, direct GroPIns sensing is demonstrated monitoring the change in SERS intensity of the prominent peaks in the GroPIns spectra as a function of its concentration, overcoming many of the limitations associated with the detection of GroPIns. More precisely, the presented SERS biosensor provides rapid (acquisition time: 1−10 s) and sensitive (detection limit: 200 nM at 10 s acquisition time) detection of GroPIns. Crucially, this allows for quantitative SERS measurements of GroPIns concentration within a mixture (*myo*-inositol and glycerol) with an accuracy of 6%. Potentially, this method could reveal the presence and concentration of this molecule in a biological sample, such as cell extracts, eliminating the need of any label or a preliminary GroPIns isolation. This possibility is of paramount relevance, in general, for SERS studies of cancer markers in cells that are difficult to isolate.

RESULTS

Substrate Description and Optical Characterization. The SERS substrates were fabricated using electron beam lithography, following a procedure similar to that reported in ref 38 and detailed in the Materials and Methods section. As visible in the photograph shown in Figure 1, each substrate hosts multiple (nine in this example) distinct, but nominally identical, sensing areas separated by 4 mm and each made of a Au-fishnet on a 25 × 25 mm^2 glass slide. Each pattern covers an area of 200 × 200 μm^2, highlighted by triangular markers for ease of operation. Figure 1 additionally shows a scanning electron microscope (SEM) picture of a typical Au-fishnet, with periodicity

p = 400 nm and wire width d = 90 nm. These parameters were found to produce the greatest enhancement factor when detecting rhodamine (Rd6G), when varying p between 100 and 500 nm and d between 30 and 90 nm. These parameters are used for the Au-fishnet substrate in the rest of this article.

We characterized the optical response of each Au-fishnet pattern, acquiring their transmission spectra. For this purpose, we used a custom-made setup described in the Materials and Methods section. In Figure 1, we show the transmission curves of a typical Au-fishnet-based SERS substrate, illuminated at normal incidence, for polarization along the major axes of the fishnet (in blue and green). As expected, the transmission is polarization independent.

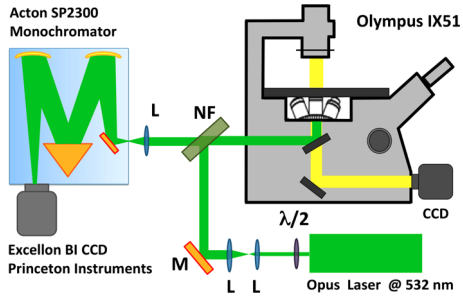

Figure 2. Schematic of our Raman microscope system. A diode laser at 532 nm is used to excite Raman scattering. The laser beam is introduced into an inverted microscope through a high numerical aperture objective (100×). The scattered light from the sample is collected by the same objective and coupled into a spectrometer equipped with a cooled CCD camera. Symbols legend: M, mirror; L, lens; NF, notch filter.

SERS Detection and Reproducibility. We performed SERS analysis using the Raman microscope shown in Figure 2. The performance of the substrates was characterized and compared to that of standard silver nanocollidal solution (Ag-NC) samples, custom-made using the procedure reported in refs 25 and 39 using the SERS signal of Rd6G in deionized water, at a concentration of 10^{-8} M, in the spectral range of 400–2000 cm^{-1}. The power of incident light was 50 μW, and the integration time was 1 s. For the Au-fishnet patterns, a drop (≈1–2 μL) of analyte was applied to the nanostructures and allowed to bind for 1 h at room temperature prior to spectrum acquisition. Conversely, a 50–60% solution of Ag-NC in deionized water was mixed with the Rd6G solution (at a final concentration of 10^{-8} M), and a drop was placed on a glass slide for the same amount of time.

For both samples, we recorded 30 spectra from different locations within each sensing area to create a statistically relevant data distribution, and we compared the results. This is the standard procedure in the Ag-NC SERS substrate, which ensures representative sampling and incorporates spot-to-spot variability in the signal. All spectra are, in a first step, baseline corrected and thereafter normalized to the maximum Raman peak (band centered at 1360 cm^{-1}). The results are shown in Figure 3a,b for the Au-fishnet and the Ag-NC, respectively. The characteristic vibrational bands of Rd6G are observed: the intense Raman bands

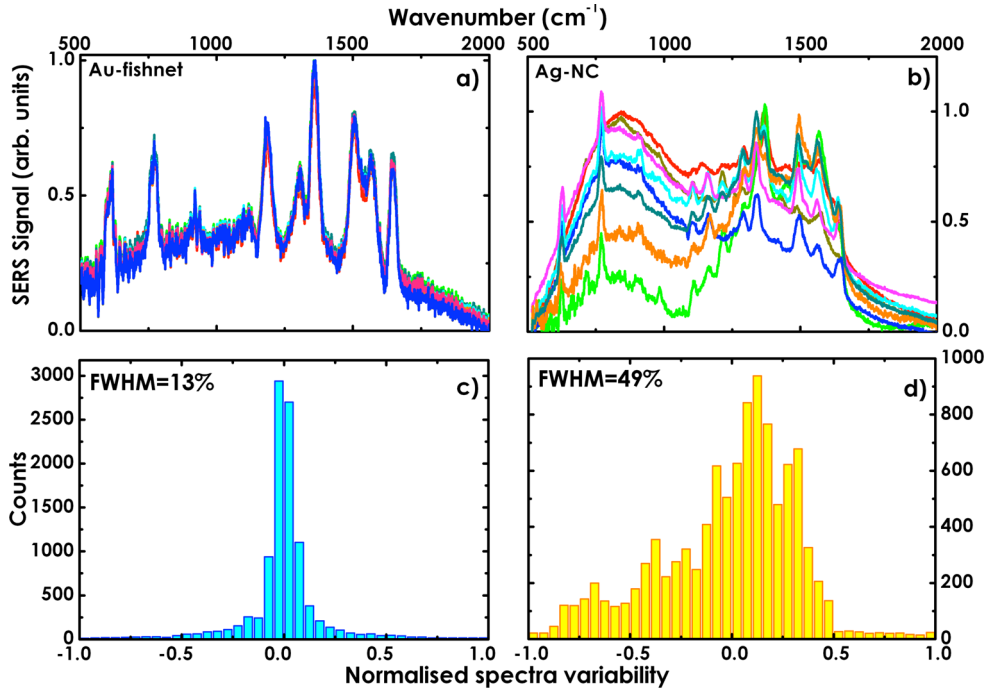

Figure 3. Randomly selected SERS acquisitions (raw data) for Rd6G samples, at a concentration of 10^{-8} M, incubated on a Au-fishnet substrate (a) and with Ag-NC (b). The average spectra normalized variability of each individual spectral distributions for SERS spectra of Rd6G on a Au-fishnet substrate (c) and in Ag-NC (d).

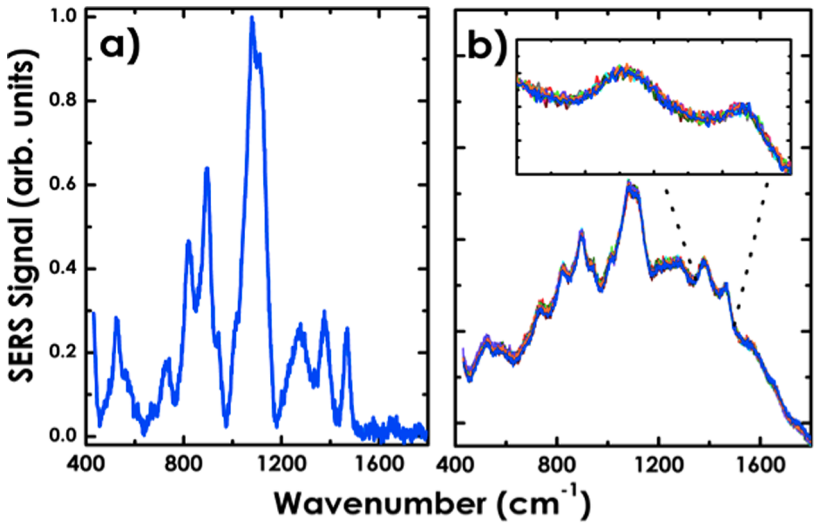

Figure 4. (a) Typical SERS signal of GroPIns at the concentration of 100 μM. (b) Ten acquisitions of the same sample in different SERS-active sites of the Au-fishnet substrate.

around 1360, 1510, and 1650 cm^{-1} can be attributed to C−C vibrations; the band at 1180 cm^{-1} can be related to C−H bending and N−H bending vibration of xanthene ring, and the peak at 1575 cm^{-1} can be attributed to C−O stretching. The SERS substrate background spectrum, before adding the dye on the SERS pattern, was also measured, showing a broad shape without any Raman bands.

We experimentally evaluated the SERS enhancement factor G for both Ag-NC and Au-fishnet substrates.[40] The highest enhancement factor experimentally observed for Au-fishnet substrates was $G_{fishnet} = 7.6 \times 10^3$. Ag-NCs show slightly higher Raman scattering enhancement: $G_{colloids} = 4 \times 10^4$. Despite the slightly reduced enhancement factor (in particular, the signal-to-noise ratio, SNR, at 1360 cm^{-1} is almost 5 times better than the Au-fishnet substrate), it is clear from this figure that the SERS signal of the Au-fishnet samples is remarkably more reproducible when compared to that of the Ag-NC case.

In order to quantify the degree of similarity of separate spectra, we evaluated the variability of each individual spectra after normalization with the average spectra. The results are arranged in the histograms represented in Figure 3c,d. The full width at half-maximum (fwhm) values for all Rd6G spectra acquired with Ag-NC and Au-fishnet substrates are, respectively, 49 and 13%. The Au-fishnet substrate shows a clearly lower fwhm value than the Ag-NC substrate, closer to the ideal case of perfect reproducibility. By increasing the laser power and integration time, a further reduction of the fwhm is observable for the Au-fishnet substrate. The same analysis performed on the Ag-NC substrate does not show a significant improvement in the reproducibility. These results demonstrate that the variability in the SERS spectra, in the case of the Ag-NC substrate, is mainly due to the variation in the relative intensities of the Raman bands more than the SNR of the SERS signal.

Additionally, experiments were repeated by comparing the spectra obtained on different days and on different sample batches. The data obtained for Au-fishnet substrates all showed consistent results; the same was not observed for Ag-NC. From the results presented here, it can be concluded that Au-fishnet substrates can be used to develop a sensitive SERS biosensing platform, especially when dealing with low concentration samples.

GroPIns Sensing. A valuable GroPIns sensor must be capable of detecting GroPIns in the 0−10 mM range close to physiological conditions with high reproducibility, low detection limit, and minimal detectable variations. The reproducibility of the SERS spectra for the GroPIns case was tested as before. Figure 4a shows a typical SERS spectrum of a GroPIns solution with concentration of 100 μM between 400 and 1800 cm^{-1}, acquired and normalized as for the Rd6G case. Figure 4b shows 10 overlapped randomly selected spectra and their zoomed-in view in the inset. The fwhm of the spectra variability for this set of measurements was about 12%, which confirms that the reproducibility is reliable also for molecules of biological relevance.

Table 1 gives most of the skeletal vibrations of GroPIns in the considered spectral region. The strong interaction between the C−C and C−O bonds gives a complex array of vibration bands, which is overlapped with the peaks arising from CH_2 vibrations. However, the SERS spectrum of GroPIns shows a very strong and specific peak centered at ∼1080 cm^{-1} that has been earlier assigned to the phosphodioxy group PO_2^-.[41]

The ability of a sensor to measure concentration is given by the noise equivalent concentration (NEC). NEC corresponds to the minimum detection limit of

TABLE 1. Band Component Analysis of the SERS Spectra of GroPIns, *myo*-inositol and glycerol in the 400−1800 cm^{-1} Wavenumber Region (Abbreviations: ν = stretch, τ = twist, δ = bend; T = trans, G = gauche)

GroPIns Raman bands (cm^{-1}) 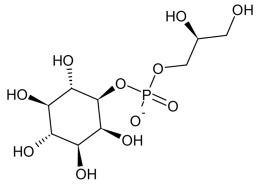	*myo*-inositol Raman bands (cm^{-1}) 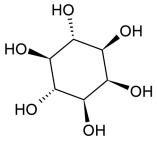	glycerol Raman bands (cm^{-1}) 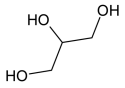	Band assignment
-	-	674	δ(CCO)+δ(OH)[43]
720	720	-	δ(CCO)[44]
815	-	821	ν(CC)[43]
-	-	850	ν(CC)[43]
895	890	-	CH_3 rock[45]
940	933	924	CH_2 rock[43]
-	-	974	CH_2 rock[43,45]
-	1005	-	$\nu(CCO)_G$[45]
-	-	1050	ν(COH) from C-1, C-3[43,46]
1071	1071	1071	$\tau(CH_2)$[46]
1080	-	-	PO_2^-[41]
-	-	1109	ν(COH) from C-2[46]
1120	1123	-	$\nu(CC)_T$
1283	1281	1252	$\tau(CH_2)$[46]
1376	1376	1357	δ(COH)[46]
1464	-	1464	$\delta(CH_2)$[46]

the system, which is the concentration at which SNR becomes equal to unity.[42] In order to estimate the detection sensitivity of the device, SERS spectra of GroPIns solutions at different concentrations (in the range between 0 and 10 mM) were acquired. The SNR of the system at each concentration was evaluated by taking the ratio of the average of peak intensity value at 1080 cm^{-1} to the standard deviation (std) of the spectral region between 1600 and 1800 cm^{-1}. Figure 5a shows the variation of SNR with GroPIns concentration in the range of 0.5−10 mM, acquired with a laser excitation power of ~50 μW and an integration time of 1 s. It can be noted that the SNR values follow a positive linear relation to the concentration of the GroPIns. The NEC was estimated, from a linear fit of the experimental data, to be 69 ± 20 μM.

Since the scattered light intensity depends on the incident laser power and the efficiency of signal collection, the NEC value can be further improved by slightly increasing the laser power on the sample (~80 μW) and the integration time (10 s). Figure 5b shows a zoom of the SNR *versus* GroPIns concentration in the range of 0−200 μM. In these experimental conditions, we demonstrate that the minimum detectable concentration is 218 ± 40 nM. This value is about 2 orders of magnitude lower than the minimum concentration expected for GroPIns in cells.[1] This is an intriguing finding in view of the quantitative detection of GroPIns

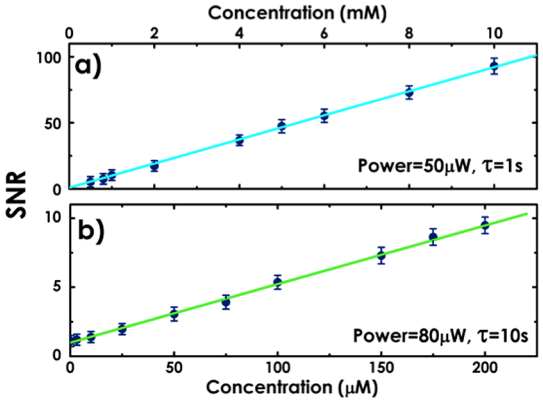

Figure 5. (a) Signal-to-noise ratio (SNR) of the peak at 1080 cm^{-1} of the GroPIns-SERS spectrum as a function of the GroPIns concentration (in the range between 0.5 and 10 mM), measured with a laser excitation power on the sample of ~50 μM and an integration time of 1 s. (b) SNR *versus* GroPIns concentration in the range between 0.25 and 200 μM, measured with a laser excitation power on the sample of 80 μW and an integration time of 10 s.

at intracellular levels. Higher powers and longer acquisition times do not improve further the NEC as it can lead to sample damage.

Quantitative Analysis of GroPIns Mixtures. To evaluate the discriminatory power of GroPIns-SERS detection, we tested a mixture of three molecular solutions (GroPIns, *myo*-inositol, glycerol), which are simultaneously present in cells and possess common chemical

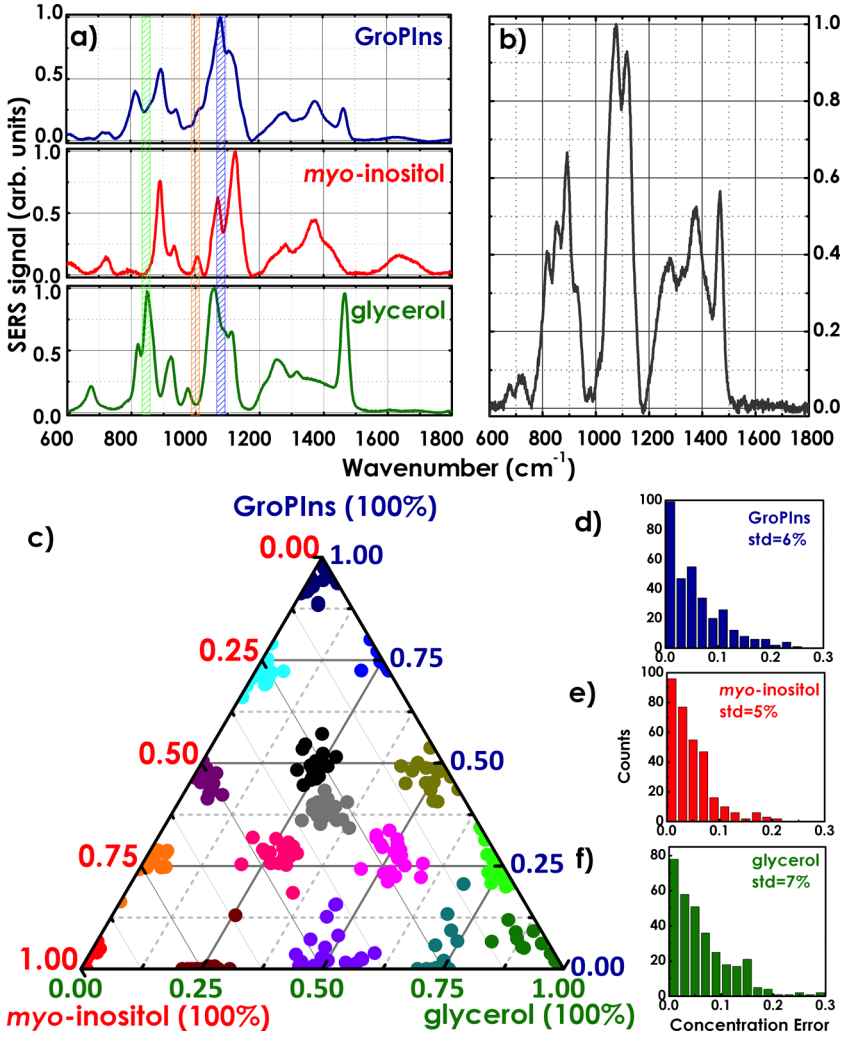

Figure 6. (a) Average SERS spectra (n = 30) from GroPIns (100 μM), *myo*-inositol (100 μM), and glycerol (100 μM). (b) SERS spectrum of the three-component mixture at the relative concentration of 33.333 μM GroPIns, 33.333 μM *myo*-inositol, and 33.333 μM glycerol. Ternary plot illustrating the composition of three-component mixtures of GroPIns, *myo*-inositol, and glycerol as measured using the leave-one-out cross-validation of the partial least-squares regression. (d–f) Histograms of the difference between the measured concentration and the nominal relative concentrations. The standard deviations of these distributions are 6, 5, and 7%, respectively.

moieties. Averaged SERS spectra (n = 30) for each molecule at a concentration of 100 μM are shown in Figure 6a. The spectra appear very similar to one another in the number and location of the peaks, albeit with notable differences in the relative intensity of some bands. Table 1 gives the skeletal vibrations of these components in the spectral region between 600 and 1800 cm^{-1}. The SERS spectrum of pure glycerol is dominated by the intense C–C stretching band at 850 cm^{-1} and CH_2 deformation vibration at 1464 cm^{-1}. The *myo*-inositol spectrum is partially overlapped to the GroPIns spectrum but shows an isolated medium intensity band at 1005 cm^{-1} assigned to C–C–O stretching. Conversely, as already stated, the GroPIns-SERS spectrum is dominated by the peak centered at ~1080 cm^{-1}, assigned to the phosphodioxy group. This variation in SERS intensity plays a critical role in determining the ability to identify the GroPIns in a mixture and therefore gauge its concentration accuracy.

The mixed samples consisted of varying concentrations of GroPIns, *myo*-inositol, and glycerol with their total concentration held constant at 100 μM. This value was chosen since the apparent intracellular GroPIns concentration is on the order of 100 μM. In Figure 6b, we report the SERS spectrum of the three-component mixture at the relative concentration of 33.333 μM.

The spectrum of the three-component mixture presents a greater challenge with respect to its interpretation and quantification. The analysis was carried out using the partial least-squares (PLS) method. The raw spectra were corrected for dark current/fluorescence background and normalized. These preliminary steps eliminate complicating contributions from variations in the baseline or slight heterogeneity in the substrate enhancement factors. PLS is a statistical technique that

determines a linear regression between the observable variables (SERS spectra in our case) and the properties that we want to measure (concentrations in our case).[47] The entire spectral range from 600 to 1800 cm^{-1} was used to build PLS models for these mixtures. The ternary plot in Figure 6c shows the relative predicted concentrations of GroPIns, *myo*-inositol, and glycerol (dots) compared to the nominal values (continuous line intersections in the equilateral triangle and the center of the triangle). The concentration of each species is 100 μM (pure phase), in correspondence of its own triangle corner, then it decreases linearly with increasing distance from this corner and reaches the value 0 on the opposite line. By drawing parallel lines at regular intervals between the zero line and the corner, fine divisions can be established for easy estimation of the content of a species. We analyzed 16 different mixtures with the same total concentration (100 μM) and various relative compositions. In each case, 1 μL of each sample was applied to the SERS substrate. The performance of the classification model was evaluated using the leave-one-out cross-validation method. To cross-validate the PLS model, 479/480th of the spectra were used to generate a PLS model and the left-out spectrum was tested as an unknown sample. This process was repeated until each sample was left out, and the results were compiled to determine the standard deviation of concentration measurements. The histograms in Figure 6d–f show the measured concentration error. From this distribution, we observe that GroPIns can be detected with an accuracy of 6%.

DISCUSSION AND CONCLUSIONS

From our analysis, we can conclude that it is not convenient to develop a single SERS substrate for every experimental condition. Attempting a rough categorization: (i) If the aim is to ascertain the presence of a given molecule in an analyte, Ag-NC substrates are the most efficient solution. (ii) For single-molecule analysis, substrates which offer a distribution of localized and very intense hot spots are the most promising approach. (iii) In a low molecular concentration regime, but where a quantitative analysis of the concentration is required, substrates like the one presented here are particularly well-suited.

The main advantage of our substrates over alternative approaches is that the relative amplitude of the Raman peaks in an acquired spectrum is consistently the same, across the sample and over extended periods of time. The same cannot be said of Ag-NC substrates, which produce a random distribution of the peak amplitudes, very different even in neighboring positions and degrading over time. This feature is crucially important when trying to measure the concentration of a molecule in a mixture containing elements with overlapping Raman spectra. Additionally, by considering the experimental conditions set in this experiment (laser wavelength, laser power, integration time, sample concentrations), we showed that our easily fabricated Au-fishnet substrate allows unprecedented reproducibility in sensing very low concentrations (200 nM) of GroPIns at a sample volume of ~1 μL and integration time of 10 s. This is the first sensitive and quantitative demonstration of the detection of GroPIns at extremely low concentration by SERS technique.

Moreover, these studies demonstrate that the proposed SERS biosensor is not only able to identify but also able to accurately and quantitatively determine the concentration of GroPIns within multicomponent mixtures. The mixed samples consisted of varying concentrations of GroPIns, *myo*-inositol, and glycerol with their total concentration held constant at 100 μM. SERS spectra were analyzed using PLS regression to extract qualitative and quantitative information regarding the composition of the mixtures. Figure 6c shows the predicted (dots) *versus* the true concentrations (triangle coordinates) for the analyzed samples. The good graphical agreement between predicted and true values is also quantified using the leave-one-out cross-validation method. Excellent accuracy (6%) in the quantification of the three component mixtures (GroPIns, *myo*-inositol, and glycerol) with similar chemical and spectral structure has been demonstrated.

The methodology described in this study should overcome many of the limitations of previous methods by providing rapid (acquisition time: 1 s), quantitative (accuracy: 6%), and sensitive detection of minimal sample concentration (detection limit: 200 nM at 10 s of acquisition time), eliminating the need of any label or dye.

These results indicate that our approach could be used as a label-free method to detect GroPIns even in cell extracts, and it may provide a novel technological platform to identify GroPIns profiles in disease pathogenesis. Further, our method is not limited to GroPIns and can be applied to a vast class of molecules, for example, to study real-time molecular dynamics in solution or on cell membranes.

MATERIALS AND METHODS

SERS Substrate Fabrication. To prepare the samples, glass substrates (thickness: 150 μm) were cleaned in acetone and isopropyl alcohol in an ultrasonic bath. A 30 nm thick film of gold was evaporated onto the glass and spin-coated with a 100 nm thick layer of SU8 (an epoxy-based negative lithographic resist from Microchem Corp.), which was baked for 5 min at 100 °C. The Au-fishnet pattern was defined by electron beam lithography, using a Raith converted Leo SEM, operating at 30 kV. The sample was then post-exposure-baked for 2 min at

100 °C before being developed in ethyl lactate solvent for 45 s. A 9 min long Ar-based reactive ion etching with a forward bias of −330 V was then used to transfer the patterns on the gold, followed by gentle O_2 ashing to remove the leftover resist.

GroPIns Preparation. GroPIns calcium salt, purified by subsequent crystallization cycles, was kindly provided by Euticals S.p.a. (Lodi, Italy). Glycerol and *myo*-inositol were from Sigma-Aldrich (Milano, Italy). They are all water-soluble and were resuspended in Milli-Q water at a concentration of 100 μM. Three component mixtures of GroPIns, *myo*-inositol, and glycerol were then prepared for analysis. The total concentration of each sample was held constant at 100 μM, but the concentration of each component was varied from 0 to 100 μM. A scheme of all the relative concentrations used in the experiment is shown in Figure 6c.

Experimental Setup for Optical Characterization of the Substrates. The experimental setup consists of a super continuum source (NKT Koheras), with controlled polarization, collimated on the sample with a 50× long working distance Mitutoyo objective (NA = 0.42). An identical objective collected the light and sent it to a CCD camera for visualization and an optical spectral analyzer (Ocean Optics USB 2000; 500−1000 nm). The light path was arranged in Köhler configuration to finely control the angle of incidence of the beam on the sample.[48]

SERS Experimental Setup. A scheme of the SERS experimental setup is shown in Figure 2. The polarization-controlled Raman probe at 532 nm (Laser Quantum, Opus, maximum Power 2 W) was first expanded by two lenses and then focused onto the sample by a 100× objective lens (Olympus, NA = 1.2), giving a laser spot on the sample of ≈0.3 × 0.3 μm^2. The back-scattered light from the sample was collected by the same objective and filtered by a holographic notch filter to remove the pump radiation. The Raman light was focused onto the entrance slit (set at an aperture of 100 μM) of the monochromator (Acton SP2300, Princeton Instruments), equipped with a 1800 lines/mm holographic grating and finally detected using a back-illuminated CCD (PIXIS:400BR-eXcelon CCD, Princeton Instruments), thermoelectrically cooled to −70 °C.

Data Analysis. The SERS enhancement factor (G) has been calculated from the enhancement of the local intensity of the incident light at the laser frequency ν_{laser} (Rayleigh scattering)[40] by using

$$G = \frac{|E_{loc}(\nu_{laser})|^4}{|E_{inc}(\nu_{laser})|^4} \quad (1)$$

In order to quantify the degree of similarity of separate SERS spectra, we calculate the average spectrum for each substrate. All the individual spectra are normalized using the average spectrum to deliver the relative variability. The fwhm of the variability histograms is used to quantify the spectral reproducibility.

Partial least-squares regression was used to quantify the presence of GroPIns in the sample mixtures. The PLS method determines the linear multivariate relationship between the observed spectra and the chemometric concentrations of the sample. In practice, this can be understood as the determination of the error-minimizing projection from the large number of measured correlated quantities (spectra) to the sparse space defined by the concentrations of the different constituents.

The PLS regression was performed on the 479 acquired spectra (16 samples × 30 acquisition minus one used for leave-one-out cross-validation). Here, we are interested in measuring the relative concentrations of the three compounds, and we have maintained a constant concentration throughout the experiments $c_1 + c_2 + c_3 = 100\ \mu$M, where c_1, c_2, and c_3 are the respective concentrations of the three compounds. We eliminate the linear interdependence between the three concentrations by representing the relative concentration in the 2D ternary plane using the relationships

$$\begin{aligned} x &= c_1 - (c_2 + c_3)/2 \\ y &= \sqrt{3}(c_2 - c_3)/2 \end{aligned} \quad (2)$$

The PLS regression was performed between this 2D space and the acquired spectra. A single spectrum was left out when determining the PLS regression and subsequently used to predict the (x,y) ternary position of the sample and deduce the respective concentrations c_1, c_2, and c_3. To statistically quantify the concentration detection error, we repeated the leave-one-out cross-validation step with each individual spectrum taken from all the acquired data. The accuracy of our procedure was determined using the classification error, that is, the difference between predicted and real concentration for each of the leave-one-out spectrum. This is represented in the histograms in Figure 6. The standard deviation (std) of these distributions quantifies the overall accuracy and precision of our detection method. The numerical procedures were implemented using the statistics toolbox in Matlab.

Conflict of Interest: The authors declare no competing financial interest.

Acknowledgment. A.C.D.L. is supported by an AIRC Start-up Grant 11454 and a FIR project RBFR12WAPY. A.D.F. is supported by an EPSRC Career Acceleration Fellowship (EP/I004602/1). D.C. is supported by an AIRC Grant IG10341 and the projects PON01-00117 and PON01-00862. S.M. is supported by a PRIN project 2012CK5RPF_05.

REFERENCES AND NOTES

1. Corda, D.; Iurisci, C.; Berrie, C. P. Biological Activities and Metabolism of the Lysophosphoinositides and Glycerophosphoinositols. *Biochim. Biophys. Acta* **2002**, *1582*, 52–69.
2. Berrie, C. P.; Dragani, L. K.; van der Kaay, J.; Iurisci, C.; Brancaccio, A.; Rotilio, D.; Corda, D. Maintenance of PtdIns45P_2 Pools under Limiting Inositol Conditions, As Assessed by Liquid Chromatography−Tandem Mass Spectrometry and PtdIns45P_2 Mass Evaluation in Ras-Transformed Cells. *Eur. J. Cancer* **2002**, *38*, 2463–2475.
3. Mariggiò, S.; Sebastià, J.; Filippi, B. M.; Iurisci, C.; Volonté, C.; Amadio, S.; Falco, V. D.; Santoro, M.; Corda, D. A Novel Pathway of Cell Growth Regulation Mediated by a PLA2α-Derived Phosphoinositide Metabolite. *FASEB J.* **2006**, *20*, 2567–2569.
4. Bos, J. L. The Ras Gene Family and Human Carcinogenesis. *Mutat. Res.* **1988**, *195*, 255–271.
5. Corda, D.; Zizza, P.; Varone, A.; Bruzik, K. S.; Mariggiò, S. The Glycerophosphoinositols and Their Cellular Functions. *Biochem. Soc. Trans.* **2012**, *40*, 101–107.
6. Patrussi, L.; Mariggiò, S.; Paccani, S. R.; Capitani, N.; Zizza, P.; Corda, D.; Baldari, C. T. Glycerophosphoinositol-4-Phosphate Enhances SDF-1α-Stimulated T-Cell Chemotaxis through PTK-Dependent Activation of Vav. *Cell Signal* **2007**, *19*, 2351–2360.
7. Patrussi, L.; Mariggiò, S.; Corda, D.; Baldari, C. T. The Glycerophosphoinositols: From Lipid Metabolites to Modulators of T-Cell Signaling. *Front. Immunol.* **2013**, *4*, 213.
8. Berrie, C. P.; Iurisci, C.; Piccolo, E.; Bagnati, R.; Corda, D. Analysis of Phosphoinositides and Their Aqueous Metabolites. *Methods Enzymol.* **2007**, *434*, 187–232.
9. Dragani, L. K.; Berrie, C. P.; Corda, D.; Rotilio, D. Analysis of Glycerophosphoinositol by Liquid Chromatography−Electrospray Ionisation Tandem Mass Spectrometry Using a β-Cyclodextrin-Bonded Column. *J. Chromatogr. B* **2004**, *802*, 283–289.
10. Petry, R.; Schmitt, M.; Popp, J. Raman Spectroscopy—A Prospective Tool in the Life Sciences. *Chem. Phys. Chem.* **2003**, *4*, 14–30.
11. Jonáš, A.; De Luca, A. C.; Pesce, G.; Rusciano, G.; Sasso, A.; Caserta, S.; Guido, S.; Marrucci, G. Diffusive Mixing of Polymers Investigated by Raman Microspectroscopy and Microrheology. *Langmuir* **2010**, *26*, 14223–14230.
12. Fleischmann, M.; Hendra, P.; Mcquillan, A. Raman Spectra of Pyridine Adsorbed at a Silver Electrode. *Chem. Phys. Lett.* **1974**, *26*, 163–166.
13. Auchinvole, C. A. R.; Richardson, P.; McGuinnes, C.; Mallikarjun, V.; Donaldson, K.; McNab, H.; Campbell, C. J. Monitoring Intracellular Redox Potential Changes Using SERS Nanosensors. *ACS Nano* **2012**, *6*, 888–896.
14. Grubisha, D.; Lipert, R.; Park, H.; Driskell, J.; Porter, M. Femtomolar Detection of Prostate-Specific Antigen: An

Immunoassay Based on Surface-Enhanced Raman Scattering and Immunogold Labels. *Anal. Chem.* **2003**, *75*, 5936–5943.
15. Ren, W.; Fang, Y.; Wang, E. A Binary Functional Substrate for Enrichment and Ultrasensitive SERS Spectroscopic Detection of Folic Acid Using Graphene Oxide/Ag Nanoparticle Hybrids. *ACS Nano* **2011**, *5*, 6425–6433.
16. Barhoumi, A.; Zhang, D.; Tam, F.; Halas, N. Surface-Enhanced Raman Spectroscopy of DNA. *J. Am. Chem. Soc.* **2008**, *130*, 5523–5529.
17. Rusciano, G.; De Luca, A. C.; Pesce, G.; Sasso, A.; Oliviero, G.; Amato, J.; Borbone, N.; D'Errico, S.; Piccialli, V.; Piccialli, G.; *et al.* Label-Free Probing of G-Quadruplex Formation by Surface-Enhanced Raman Scattering. *Anal. Chem.* **2011**, *83*, 6849–6855.
18. Rusciano, G.; De Luca, A. C.; Pesce, G.; Sasso, A. On the Interaction of Nano-sized Organic Carbon Particles with Model Lipid Membranes. *Carbon* **2009**, *47*, 2950–2957.
19. Garrell, R. Surface-Enhanced Raman Spectroscopy. *Anal. Chem.* **1989**, *61*, n401A–411A.
20. Moskovits, M. Surface-Enhanced Spectroscopy. *Rev. Mod. Phys.* **1985**, *57*, 783–826.
21. Kamnhampati, P.; Child, C.; Foster, M.; Campion, A. On the Chemical Mechanism of Surface Enhanced Raman Scattering: Experiment and Theory. *J. Chem. Phys.* **1998**, *108*, 5013–5026.
22. Dinish, U.; Yaw, F.; Agarwal, A.; Olivo, M. Development of Highly Reproducible Nanogap SERS Substrates: Comparative Performance Analysis and Its Application for Glucose Sensing. *Biosens. Bioelectron.* **2011**, *26*, 1987–1992.
23. Huh, Y. S.; Chung, A. J.; Erickson, D. Surface Enhanced Raman Spectroscopy and Its Application to Molecular and Cellular Analysis. *Microfluid. Nanofluid.* **2009**, *6*, 285–297.
24. Anker, J. N.; Hall, W. P.; Lyandres, O.; Shah, N. C.; Zhao, J.; Van Duyne, R. P. Biosensing with Plasmonic Nanosensors. *Nat. Mater.* **2008**, *7*, 442–453.
25. Lee, P.; Meisel, D. Adsorption and Surface-Enhanced Raman of Dyes on Silver and Gold Sols. *J. Phys. Chem.* **1982**, *86*, 3391–3395.
26. Weitz, D.; Gramila, T.; Genack, A.; Gersten, J. Anomalous Low-Frequency Raman Scattering from Rough Metal Surfaces and the Origin of Surface-Enhanced Raman Scattering. *Phys. Rev. Lett.* **1980**, *45*, 355–358.
27. Wang, H.; Brandl, D.; Nordlander, P.; Halas, N. Plasmonic Nanostructures: Artificial Molecules. *Acc. Chem. Res.* **2007**, *40*, 53–62.
28. Schlücker, S. SERS Microscopy: Nanoparticle Probes and Biomedical Applications. *Chem. Phys. Chem.* **2009**, *10*, 1344–1354.
29. Shanmukh, S.; Jones, L.; Driskell, J.; Zhao, Y.; Dluhy, R.; Tripp, R. Rapid and Sensitive Detection of Respiratory Virus Molecular Signatures Using a Silver Nanorod Array SERS Substrate. *Nano Lett.* **2006**, *6*, 2630–2636.
30. Baia, L.; Baia, M.; Popp, J.; Astilean, S. Gold Films Deposited Over Regular Arrays of Polystyrene Nanospheres as Highly Effective SERS Substrates from Visible to NIR. *J. Phys. Chem. B* **2006**, *110*, 23982–23986.
31. Liu, G.; Lee, L. Nanowell Surface Enhanced Raman Scattering Arrays Fabricated by Soft-Lithography for Label-Free Biomolecular Detections in Integrated Microfluidics. *Appl. Phys. Lett.* **2005**, *87*, 074101.
32. Zhang, X.; Whitney, A.; Zhao, J.; Hicks, E.; Van Duyne, R. P. Advances in Contemporary Nanosphere Lithographic Techniques. *J. Nanosci. Nanotechnol.* **2006**, *6*, 1920–1934.
33. Liu, H.; Zhang, L.; Lang, X.; Yamaguchi, Y.; Iwasaki, H.; Inouye, Y.; Xue, Q.; Chen, M. Single Molecule Detection from a Large-Scale SERS-Active $Au_{79}Ag_{21}$ Substrate. *Sci. Rep.* **2011**, *1*, 112.
34. Lee, H. M.; Jin, S. M; Kim, H. M.; Suh, Y. Single-Molecule Surface-Enhanced Raman Spectroscopy: A Perspective on the Current Status. *Phys. Chem. Chem. Phys.* **2013**, *15*, 5276–5287.
35. La Ru, E. C.; Etchegoin, P. G. Single-Molecule Surface-Enhanced Raman Spectroscopy. *Annu. Rev. Phys. Chem.* **2012**, *63*, 65–87.
36. Perney, N. M. B.; Baumberg, J. J.; Zoorob, M. E.; Charlton, M. D. B.; Mahnkopf, S.; Netti, C. M. Tuning Localized Plasmons in Nanostructured Substrates for Surface-Enhanced Raman Scattering. *Opt. Express* **2006**, *14*, 847–857.
37. Jiao, Y.; Ryckman, J. D.; Ciesielski, P. N.; Escobar, C. A.; Jennings, G. K.; Weiss, S. M. Patterned Nanoporous Gold as an Effective SERS Template. *Nanotechnology* **2011**, *22*, 295302.
38. Di Falco, A.; Ploschner, M.; Krauss, T. F. Flexible Metamaterials at Visible Wavelengths. *New J. Phys.* **2010**, *12*, 113006.
39. Rusciano, G.; De Luca, A. C.; D'alessio, A.; Minutolo, P.; Pesce, G.; Sasso, A. Surface-Enhanced Raman Scattering Study of Nano-sized Organic Carbon Particles Produced in Combustion Processes. *Carbon* **2008**, *46*, 335–341.
40. Zhang, W.; Fischer, H.; Schmid, T.; Zenobi, R.; Martin, O. J. F. Mode-Selective Surface-Enhanced Raman Spectroscopy Using Nanofabricated Plasmonic Dipole Antennas. *J. Phys. Chem. C* **2009**, *113*, 14672–14675.
41. Krafft, C.; Neudert, L.; Simat, T.; Salzer, R. Near Infrared Raman Spectra of Human Brain Lipids. *Spectrochim. Acta, Part A* **2005**, *61*, 1529–1535.
42. Ashok, P. C.; De Luca, A. C.; Mazilu, M.; Dholakia, K. Enhanced Bioanalyte Detection in Waveguide Confined Raman Spectroscopy Using Wavelength Modulation. *J. Biophotonics* **2011**, *4*, 514–518.
43. Mendelovici, E.; Frost, R. L.; Kloprogge, T. Cryogenic Raman Spectroscopy of Glycerol. *J. Raman Spectrosc.* **2000**, *31*, 1121–1126.
44. Yang, H.; Yang, Y.; Yang, Y.; Liu, H.; Zhang, Z.; Shen, G.; Yu, R. Formation of Inositol Hexaphosphate Monolayers at the Copper Surface from a Na-Salt of Phytic Acid Solution Studied by *In Situ* Surface Enhanced Raman Scattering Spectroscopy, Raman Mapping and Polarization Measurement. *Anal. Chim. Acta* **2005**, *548*, 159–165.
45. Joa, S. L.; Pemberton, J. E. A Surface Enhanced Raman Scattering Investigation of Interfacial Structure at Silver Electrodes in Electrolyte Solutions of the Isomers of Butanol. *Langmuir* **1992**, *8*, 2301–2310.
46. Mudalige, A.; Pemperton, J. E. Raman Spectroscopy of Glycerol/D_2O Solutions. *Vib. Spectrosc.* **2007**, *45*, 27–35.
47. Driskell, J.; Primera-Pedrozo, O.; Dluhy, R.; Zhao, Y.; Tripp, R. Quantitative Surface-Enhanced Raman Spectroscopy Based Analysis of MicroRNA Mixtures. *Appl. Spectrosc.* **2009**, *63*, 268A–286A.
48. Hammond, C. A Symmetrical Representation of the Geometrical Optics of the Light Microscope. *J. Microscopy* **1998**, *192*, 63–68.